Measurement
Manuscript Draft

Manuscript Number: MEAS-D-18-00759

Title: Integrated Scientific Investigations On Constitutive Materials From Me-taw-ya Temple (n.1205a), Pagán Valley (Birmani)

Article Type: VSI: MetroArchaeo2017

Keywords: Bricks; Mortars; Stuccoes; Mineralogy; Provenance; Statistical treatment; Optical Microscope; EDXRF; FT-IR; XRD; TGA

Abstract: On August 24, 2016, a strong earthquake struck central Birmani. Pagán Archaeological Zone suffered extensive damage. A post-earthquake damage assessment survey was carried out from Tokyo National Research Institute for Cultural Properties. As a part of the same project, a diagnostic research was carried out to acquire information on temple Me-taw-ya located in the archaeological area. The aim of the work was to acquire information on the constitutive materials and construction technology, i.e. compositions of bricks, mortars and stuccoes.
On a preliminary phase, non-invasive ED-XRF fluorescence investigations were carried out on the pagoda exterior walls. On the basis of the results some representative samples were collected. Therefore optical microscopy observations, FT-IR, XRD and TG analyses were performed to identify the mineralogical and chemical composition of the materials. Principal component analysis (PCA) and hierarchical cluster analysis (HCA) were also performed on EDXRF chemical compositional data in order to discriminate the different materials.

Highlights:

Constitutive Materials from Me-taw-ya Temple (n.1205a), Págan Valley (Birmani)" were studied for the first time.

Principal component analysis (PCA) and hierarchical cluster analysis (HCA) performed on EDXRF chemical compositional data allowed to preliminary discriminate the different materials.

EDXRF analysis can be combined with mineralogical and petrographic investigations to obtain compositional information and to define the existence of compositional groups.

Integrated Scientific Investigations On Constitutive Materials From Me-taw-ya Temple (n.1205a), Pagán Valley (Birmani)

Maria Letizia Amadori[1], Paola Fermo[2], Valentina Raspugli[1], Valeria Comite[2], Francesco Maria Mini[1], Yoshifumi Maekawa[3], Mauro La Russa[4]

[1]*Department of Basic Sciences and Fundamentals, University of Urbino, Urbino (Italy)*
[2]*Department of Chemistry, University of Milan, Milan (Italy)*
[3]*Tokyo National Research Institute for Cultural Properties, Tokyo (Japan)*
[4]*Department of Biology, Ecology and Earth Sciences, University of Calabria, Rende, Italy*

Abstract **-** On August 24, 2016, a strong earthquake struck central Birmani. Pagán Archaeological Zone suffered extensive damage. A post-earthquake damage assessment survey was carried out from Tokyo National Research Institute for Cultural Properties. As a part of the same project, a diagnostic research was carried out to acquire information on temple Me-taw-ya located in the archaeological area. The aim of the work was to acquire information on the constitutive materials and construction technology, i.e. compositions of bricks, mortars and stuccoes.
On a preliminary phase, non-invasive EDXRF fluorescence investigations were carried out on the pagoda exterior walls. On the basis of the results some representative samples were collected. Therefore optical microscopy observations, FT-IR, XRD and TG analyses were performed to identify the mineralogical and chemical composition of the materials. Principal component analysis (PCA) and hierarchical cluster analysis (HCA) were also performed on EDXRF chemical compositional data in order to discriminate the different materials.

Keywords: Bricks; Mortars; Stuccoes; Mineralogy; Provenance; Statistical treatment; Optical Microscope; EDXRF; FT-IR; XRD; TGA

INTRODUCTION

Pagán, called Bagan too, is an ancient city located in the Mandalay Region of Birmani. It is one of Asian most important Buddhist sites and up until today it is an important centre of Theravada Buddhism. From 1044 to 1287, Pagán was the capital as well as the political, economic and cultural nerve centre of the Pagán Empire. During the kingdom over 10,000 Buddhist temples, pagodas and monasteries as well as enormous stucco-covered structures, were constructed in an area of 104 square kilometres in the Pagán plains. The remains of over 2200 temples and pagodas still survive

to the present day and they are venerated by the local population as well as by pilgrims coming from foreign countries too.
The magnificent architecture of pagodas in Pagán proves the achievement of Birmani craftsmen [1]. Fired bricks and mortars were used to build most of the temples in Pagán ; whitish stuccoes covered and decorated the exterior surfaces of the walls that today are partially detached and destroyed but, despite this, wall paintings still decorate the interior walls of many of the temples.
A strong earthquake occurred in July 1975 destroying a lot of monuments [2] and on 24 August 2016 a further magnitude 6.8 earthquake struck again central Birmani. Pagán Archaeological Zone suffered extensive damage and more than 300 structures were partially destroyed.
After the earthquake, Department of Archaeology, Japan International Cooperation Agency and the UNESCO Bangkok Office collected information about the damage to cultural heritage. Furthermore, Tokyo National Research Institute for Cultural Properties (TNRICP) carried out a post-earthquake damage assessment survey carried out in order to investigate the state of conservation of Pagán religious buildings [3].
Me-taw-ya temple (n. 1205a) is one of the temples involved in this project (fig. 1). The temple, dating XIII century, belongs to Pagán Dynasty and it is located in the middle of the Pagán Chauk Road, which connects Old Pagán and New Pagán , in the south of Myinkaba village in Pagán site.
Constitutive materials and executive techniques are the ones traditionally used in Pagán . Temple's foundation are multi-layered, approximately three meters deep: directly in contact with soil a first layer of sand and petrified wood (woodstone) was applied; above it a second layer of lime sand and broken terracotta; a third final layer was made out of lime, sand and limestone.
Both internal and external walls are constituted of fired bricks, joined using joint mortars composed of fresh clay/mud, organic binders such as sap plant and/or molasses, and sand. Building mass/core between external and internal walls are constituted of mud/clay and broken bricks.
External renderings are characterized by two different layers: the inner one are made out of lime and organic additives mixed with large-grained sand; a second outer layer is made using a finer-grained sand to achieve a polished surface. Finally, those external surfaces were further polished using washes of lime putty mixed with organic additives.
External decorations were carved in mortar-based stucco, whose constituting materials are lime, organic based materials and rough grained-sand. They were originally treated with a lime putty paste finishing – now deteriorated - and probably decorated with pigments. Traces of carbon are probably derived from the slacking process of lime. Even if executive techniques are still unclear, it is possible that some stucco mouldings were first carved, then mortared onto the external renderer and walls using the natural ledges of bricks as resting ledges to hold them in place [4]. Wall paintings with geometric designs, vegetal, circular and diamonds patterns decorate the plasters of interior walls and ceilings, containing two Buddhist statues.
The Me-taw-ya temple was already submitted to previous invasive conservation interventions, probably related to the beginning of the 19th century and to 1975 earthquake. The restoration interventions were managed without a rigorous methodology: on the exterior walls different materials, sometimes not suitable, were used and several invasive rebuilding and reconstruction were led, empirically detected, since no documentation is available [4].
Me-taw-ya pagoda was finally seriously damaged again by 2016 earthquake.

GEOGRAPHICAL AND GEOLOGICAL CONTEXT

The site of Pagán is located in the Central Birmani on the banks of the Irrawaddy River, the largest river of Birmani. The Irrawaddy waters flow down the Eastern Tibetan Plateau and the Sino-Burman Ranges on the eastern side of the Central Birmani Basin while its largest tributary, the Chindwin River, flows down the Indo-Burman Ranges. After the confluence with the Chindwin River, the course of the Irrawaddy River continues relatively straight North-South through the country, flowing into the Andaman Sea. Its drainage basin covers in total about 404200 square kilometres.

From a geological point of view, Pagán is located in the Central Birmani Basin (fig. 2), a forearc basin formed during northeastward subduction of the Bengal oceanic crust beneath Birmani [5].

The Central Birmani Basin comprises two lateral troughs of Cenozoic pullapart sub-basins, including the western Minbu Sub-Basin and the eastern Pegu Yoma Sub-Basin [6].

The Sino-Burman Ranges represents the eastern edge of central Birmani, comprising the Tenasserim highlands, the Shan Plateau and the Yunnan highlands, that are local units of the Sibumasu Terrane (eastern unit of the Indochina Peninsula) [7]. These units mainly consist of Paleozoic to Cretaceous metasediments and plutons [8].

Between the Sino-Burman Ranges and the Central Birmani Basin, the basement of the Burma Terrane crops out as belts of metamorphic rocks: the Slate and the Mogok Metamorphic Belts in the south and the Gaoligong Belt in the north [9] [10].

These belts are intruded by young batholiths and related volcanic rocks (mostly <150 Ma), including the lavas and plutons of the Wuntho-Popa Arc, which is considered as the eastern continuation of the Transhimalayan Arc of Tibet and contains relics of the Andean-type volcanic arc of the Indo-Asian subduction zone [11] [12] [13] [14].

At the western edge of Birmani, the Central Birmani Basin is separated from the Bengal fan by the Indo-Burman Ranges, which form a Cenozoic accretionary complex produced during the subduction of the Indian plate beneath the Burma Terrane [15].

METHODS AND MATERIALS

The research focused on bricks, stuccoes and mortars including both original and probably non-original materials. A first phase of non-invasive analysis was performed *on situ* on the constitutive materials with the aim of acquire preliminary information on the constituting elements of the investigated areas.

Twenty-third samples were subsequently collected (Table 1) in the external facades of temple n.1205a in order to submit them to a set of micro-invasive investigations on properly prepared samples (fig. 3).

The following analytical techniques were applied:

- EDXRF spectrometer (EDXRF)

Energy Dispersive X-ray Fluorescence analysis was carried out using an Oxford Instruments X-Met

8000 energy dispersive handheld spectrometer, with X-Flash SDD detector, 6 mm diameter spot, a Rh target X-ray tube operating both at 8 kV, 50 μA and 40 kV, 8 μA. The first operating condition is particularly sensitive to light elements (from about Al), the second to heavier ones including Sn, Sb and Ba K-lines. Measurement time was 100 s: 74 s at 8 kV and 26 s at 40 kV. Data were processed using proper software like Artax. Ten measurement points were performed for each investigated area.

- Optical microscopy (OM)

Polarization microscopy observations were performed, using transmitted light, on thin polished sections of bricks, mortars and stuccoes with a BX51 Olympus instrument polarized light, with fixed oculars of 10× and objectives with different magnifications (5, 10, 20, 50 and 100×). The minerals were identified by means of their typical birefringence and focusing the textural features.
Microscope was directly connected to an Olympus SC50 camera and to Stream Basic software for images acquisition.

- Scanning electron microscopy coupled with energy dispersive X-ray (SEM-EDS)

Morphological observations and chemical microanalyses were carried out on thin polished sections. A Hitachi Tabletop TMT3030 Electron Scanning Microscope (SEM) equipped with an energy dispersive X-Ray spectrometer (EDS) and dedicated software Quantax 70 was used. The analyses were carried out at acceleration voltage 20 kV beam current 23–25μA, with a variable working distance (from 7.3 to 11.4 mm).

- X-ray diffractometer (XRD)

Crystalline phase composition was determined by X-ray diffraction (XRD) on powders samples (bricks, mortars and stuccoes) by means of a Philips PW 3710 diffractometer continuous scanning filter with nickel using a randomly oriented powder mount and a PW1830/40 diffractometer continuous scanning filter with nickel. On the basis of the x-ray diffraction methods, major, minor and trace crystalline phases (Kretz, 1983) were calculated qualitatively with the DIFFRAC.EVA and CM stich (USB) software.
The analysis was carried out with the following conditions: emission radiation CuKα, voltage 40 kV, intensity 40 mA, goniometer speed 0.1 2 h/s.

- Thermogravimetric analyzer (TGA)

TG analyses were carried out on a selected group of samples by a Mettler Toledo TGA/DSC 3+ instrument, which allows simultaneous TG and DSC analyses. The analyses were conducted in the range 30°- 800° C, increasing the temperature with a rate of 20° C/minute, using about 2.5 mg of sample for each analysis.

- Infra red spectrophotometer (FT-IR)

FT-IR/ATR spectra were collected on bricks, mortars and stuccoes with a spectrophotometer Nicolet 380 (Thermo Electron Corporation) equipped with ATR accessory Smart Orbit and interfaced with a microscope FT-IR Nicolet Centaurus. The ATR accessory is equipped with a diamond crystal. FT-IR spectra were acquired in the range 400-4000 cm^{-1}.

- Statistical Data treatment

XRF data were treated by means of chemometric analytical techniques, such as principal component analysis (PCA) and hierarchical cluster analysis (HCA). In particular, PCA and HCA were applied considering as variables the signals intensity of XRF spectra. All the graphs reported

in the text (scatter plots and two dendrograms) were realised by using the statistical packages Minitab Inc. 15.1 and STATISTICA 7.1. PCA was carried out on the data covariance matrix.

RESULTS

A. Bricks

Non-invasive XRF analyses (Table 1s), carried out on bricks, both original and not, detected different ratio of their constitutive elements: in original bricks (MY1, MY10, MY17.3, MY50) high amounts of silicon and iron, with lower and variable concentrations of potassium, calcium, titanium, aluminium were revealed. MY17.3 and MY50 appear to be richer in calcium. Low amounts of aluminium, strontium, manganese, zirconium and variable sulphur amounts were detected too, with traces of chlorine and phosphorous. Non-original bricks (M1 ad M2) are richer in silicon, followed by iron and potassium. If compared with original bricks, calcium is lower, titanium and aluminium amounts are higher and no sulphur was detected. Low amounts of zirconium, strontium and manganese were revealed as well as chlorine traces.

Optical microscopy observations (table 2) carried out on original bricks thin sections (i.e. MY1, MY10 and MY17.3) disclose inhomogeneous colours ranging from brown/brownish red to ochre. The groundmass, consisting of clay minerals sometimes probably dehydrated, shows optical properties ranging from anisotropic to semi-isotropic (fig. 4a, 4b, 4c). The a-plastic fraction grain size ranges from 63 μm to 125 μm. A–plastic modal (volume) percentage [16] is about 10-20 % and it is composed of mono- and polycrystalline coarse quartz, biotite, alkali feldspars, fibrous muscovite, opaque minerals (iron oxides) and clinopyroxene. The coarser grains (> 125 μm) are scarce (volume percentage < 5 %) and they are mostly composed of quartz, biotite and argillaceous rock fragments. The voids percentage has amounts of about 5 %.

SEM morphological investigations and EDS elemental chemical microanalysis, performed on brick's body matrix (MY1, MY10, MY17.3) revealed a clay minerals-based matrix with high content of silicon and aluminium with lower amounts of potassium, iron, magnesium, calcium and traces of sodium (fig. 4d). Zirconium silicate particles were found too, as well as silicon and aluminium-based particles, with iron, potassium, calcium, magnesium and sodium, and titanium.

XRD analysis has confirmed the presence of the mineral phases observed by optical microscope, allowing to distinguish the presence of illite in the clay matrix. The presence of illite has been highlighted and confirmed by FT-IR analysis: the two signals related to this mineral are present in the spectra acquired on the original bricks MY17.3 and MY50 (at 1455 cm^{-1} and 1620 cm^{-1}[17]; together with the signals of calcium carbonate at about 1420 cm^{-1} (fig. 4e). It is worth noting that in case of sample MY10, in accordance with XRD data (table 3, fig 4f) the signals attributed to illite have not been identified by FT-IR analysis.

Non-original brick thin sections show a colour ranging from yellowish-brow to reddish-dark brown and the groundmass optical properties are semi-isotropic. The a-plastic inclusions have a prevalent grain size from 63 μm to 250 μm (fine sand) with some quartz and K-feldspars coarser grains (fig. 5a, 5b). A–plastic volume percentage is about 20-25% and it is composed of mono- and polycrystalline coarse quartz, cristobalite, biotite, alkali feldspars and plagioclase, rare lamellar calcic amphiboles, fibrous muscovite, opaque minerals (iron oxides) and rock fragments (i.e.

quartzite). The voids percentage is about 10-15%.
SEM-EDS investigations confirmed that brick's matrix (M1, M2) is silicon and aluminium based, with iron and lower amounts of potassium, magnesium and calcium (fig. 5c). Rare particles with high copper amounts and tin were clearly identified; other particles revealed traces of rare hearths (cerium, lanthanum, neodymium, praseodymium), vanadium, silver, chromium and phosphorous (fig. 6a, 6b). Iron-rich particles were identified as well.
Also in this case XRD (Table 3, fig, 5d) confirms the observations carried out by OM. Anorthite as plagioclases and diopside as clinopyroxene was identified while illite has never been detected.
By TGA only an initial (100-300 °C) weight loss (about 3-4%) has been highlighted on bricks samples and it is probably due to loss of hydration water present in the silicates structures.

B. Stuccoes

On the basis of ED-XRF analysis (Table 1s), the original stuccoes (MY3, MY8, MY9, MY14, MY15, MY16) are composed of calcium and silicon as main chemical elements, followed by potassium, iron, strontium, nickel, titanium, zirconium, low amounts of sulphur, traces of aluminium, manganese, chlorine and phosphorous. In non-original stuccoes (MY11 and MY12), calcium and sulphur were detected together with silicon, potassium and iron. Iron amounts are lower, if compared with original stuccoes; chlorine and nickel are higher, a slight increase in strontium and titanium signal was detected too. Traces of manganese and phosphorous were revealed as well.
Polarized optical microscope observations of the stucco samples (Table 2) show a light brown colour (fig. 7a) and the presence of an inhomogeneous texture with a very heterogeneous composition. Groundmass has a prevailing calcic composition, micritic texture and greyish-light brown colour. A-plastic grain size ranges from few μm to 500μm, with rare coarser grains. The skeleton has a silicate composition. Among the non-plastic inclusions, mono- and polycrystalline quartz is the most widespread phase, often presenting undulose extinction. Quartz grain size is very variable, reaching 1 mm in diameter. The other main phases composing the aggregate are, in decreasing order of abundance: K-feldspars (orthoclase and microcline) plagioclase, clinopyroxene, Ca-amphibole, opaque minerals and garnet. Grog, stone fragments (quartzite and limestone) were detected. Traces of bioclasts (radiolaria, shells and vegetal frustules) are also present. Inclusions volume percentage is about 20-30%. Percentage of voids is about 5-10%. Macro-porosity is mainly given by sub-rounded micro-vacuoles.
In MY15 sample, two layers were identified (Table 2, fig 7b). The outer layer is mainly composed by a dark semi-isotropic carbonate/silicate matrix surrounding angular coarse carbonate grains (calcite). Regarding the inner layer, it is quite similar to the samples described above.
In the samples MY8, MY9 and MY11 as highlighted by the FT-IR spectra (fig. 7c) the carbonate signal at about 1420 cm^{-1} was detected.
XRD analysis (Fig. 7d, Table 3) confirms the petrographic observations. Calcite is the main mineral phase followed by quartz.
SEM morphological investigations and EDS elemental chemical microanalysis (MY3, MY8, MY15, MY16 outer stucco; MY9, MY14 inner stucco), pointed out samples composition and

provided information on their inner morphology. Investigated samples are characterized by a mainly Ca-based matrix with variable silicon levels and lower amounts of magnesium, aluminium, iron, chlorine, sodium and potassium; traces of sulphur, chlorine, phosphorous, zirconium were revealed as well.
Rare particles characterized by high copper contents and secondly tin, as well as by Ba-feldspars, were found (MY3). Carbonate coarse grains were identified as well as silicate phases referable to plagioclases with albitic composition, ilmenite and titanite, K-feldspar (probably orthoclase), quartz, biotite in MY8.
Traces of chlorine, maybe referred to the matrix, were diffusely detected in MY8 sample. Areas rich in Cr in association with Fe were detected in MY9.
SEM observations of MY14 and MY15 samples pointed out the presence of a carbonate matrix with lower percentage of magnesium, aluminium, sulphur, iron, traces of sodium and potassium. A silicate phase (micaceous) in MY14 sample was identified. MY15 revealed a non-homogeneous composition with an internal matrix characterized by a prevailing silicon binder (probably mud or clay) with a lower carbonate component. Iron oxides were revealed as well as silicate phases referable to horneblende, orthoclase feldspar, quartz coarse grain, dark micas, clinopyroxenes and coarse calcite crystals.
In MY11 and MY12 samples, EDS revealed a mainly Ca-based matrix with variable silicon and magnesium as well as traces of aluminium, iron, and potassium. Quartz, iron oxides and Ti-rich particles (rutile) were detected, as well as silico-aluminates, zircon and iron-oxides particles. Traces of silver were revealed in both MY11 and MY12 samples.
In MY12 sample, EDS elemental map pointed out the presence of gypsum, maybe referable to some restoration intervention (fig 8a, 8b, 8c, 8d, 8e)
Sulphur was also detected in sample MY12 whose presence is attributable to gypsum also confirmed by XRD, FT-IR (Table 3) and SEM/EDS (fig. 8e, 8f).
TGA analyses of stuccoes samples have shown a weight loss (between 650 and 800 °C) due to calcium carbonate decomposition. The samples are quite homogeneous and on average calcium carbonate concentration is of 37%.

C. Mortars

On the basis of ED-XRF investigations carried out on some of the original mortars (MY7, MY17), high silicon and calcium amounts were revealed, followed by iron and potassium (i.e. in MY7, MY17). Low amounts of titanium, aluminium, strontium, low but variable amounts of manganese and traces of sulphur, chlorine, phosphorous and zirconium were detected too. Non-original mortars (MY4, MY5, MY6, MY13 MY17.1 and MY17.2), if compared with the original ones, are poorer in silicon, iron and potassium, and they have lower variable titanium, strontium, zirconium and nickel amounts. Aluminium was detected only in traces, as sulphur, manganese, chlorine, nickel, phosphorous.
Concerning mineralogical and petrographic observations (Table 2), in the original mortars (MY7, MY17, MY2B samples) a silicate binder was detected instead of a carbonate binder, as confirmed by SEM-EDS carried out on MY7 and MY17 that revealed a mainly silicate matrix with iron, potassium and magnesium lower amounts, calcium and sodium traces. Quartz, silico-aluminates

(spinels), Ti and Zr-rich particles, iron oxides, were detected as well. XRD (Table 3), FT-IR and TGA analyses further confirmed these results. Traces of silver and rare earths (lanthanum, cerium, praseodymium) were revealed in MY7 (Fig. 9a, 9b).
Some IR spectra acquired on original mortars (fig. 10a) clearly do not show the carbonate signal at about 1420 cm^{-1}.
The second mortar typology (MY4, MY5, MY6, MY13, MY17.1, MY17.2) shows a carbonate binder associated with a silicate phase (Table 2). The aggregate is poorly sorted and shows a rather inhomogeneous distribution. Grain size ranges from 63 μm to 1 mm with a prevalence of medium-sand-like grains. Quartz is the most represented crystalline phase; K-feldspar (orthoclase and microcline), plagioclase, Na-pyroxene, amphibole, opaque minerals (magnetite and ilmenite), epidote, titanite and micas were detected too. Fragments of limestone, shells and well-preserved vegetal frustules were also detected. Coarser inclusions are represented by grog composed of brownish clay matrix and angular fine a-plastic grain. The inclusion in these fragments has a grain-size ranging in the very-fine sand field (63-125 μm). The most represented crystalline phases are quartz, muscovite, biotite, plagioclase and Ca-amphibole. The porosity is relatively high. Inclusions volume percentage ranges from 15 to 25 %.
It is also worth noting that by FT-IR it is possible to highlight the samples inhomogeneity. In fact, while from XRD data (Table 3) MY13 and MY17.1 seem to show the same quantity of calcium carbonate, form FTIR spectra (fig. 10b) the intensity of $CaCO_3$ signal is significantly higher in the case of sample MY17.1.
OM observations of MY4 sample pointed out the presence of three different levels: the inner one (level 0) is light-coloured and rich in coarse particles; level 1, compared to the one previously described, is poor in aggregate and it seems to be more compact and homogeneous. The outer level (level 2), as level 1, is rich in aggregate but it does not seem to be compact as level 0 and 1.
SEM-EDS investigations, carried out on non-original mortar, revealed a non-homogeneous matrix composition: in some areas high silicon amounts were revealed, followed by potassium, aluminium, calcium, magnesium lower rates and sodium traces; other elements could be related to aluminosilicates in analysed area. Microanalysis carried out on a further matrix area detected high calcium amounts and, in decreasing abundance order, silicon, magnesium, aluminium and potassium content. It should be noticed that in this sample several titanium-rich particles (titanite in association with ilmenite) were identified, maybe referred to titaniferous sand. Quartz and K-feldspars were found too.
It should be noticed that in MY6 and MY17.1 several titanium-rich particles (titanite in association with ilmenite) were identified, maybe referred to titaniferous sand. Quartz, K-feldspars, Zr-rich particles were identified as well (MY13 and MY16 samples). Non-original mortars contain traces of silver and rare earths (lanthanum, cerium) (fig. 9c, 9d).
TGA analyses acquired on original mortars have not shown the presence of calcium carbonate while in the case of not original mortars the concentration of $CaCO_3$ ranges from 8 to 16% (between 650 and 800 °C).

DISCUSSION

A. Bricks

The mineralogical, petrographic and textural characterization of the bricks (Table 2) together with XRD data (Table 3) allowed distinguishing the original ones from those probably employed in a restoration intervention.

Particularly mineral compositions, grain size distribution, porosity and clay matrix optical properties are the features that allow to clearly distinguish the two bricks groups. Some of these differences could be related to different thermal treatments for original vs non-original bricks.

The original brick (bricks I: MY1, MY10, MY17.3, MY50 samples) matrix shows anisotropic optical properties, allowing to estimate a lower firing temperature. SEM morphological investigations and EDS elemental chemical microanalysis on original brick's body matrix pointed out the presence of a mainly silicate matrix (illite/smectite clay minerals) confirmed by XRD. The presence of chlorite in two original bricks, detected by X-ray diffraction, allows to suppose a heating temperature not exceeding ~725°C. In fact, chlorite begins to decompose at ~550 °C and disappears at 725 °C [21].

On the contrary, isotropy of non-original bricks (bricks II: M1, M2 samples) matrix is the evidence of the highest reached temperatures. In fact ceramic fired in the temperature range of 700-850°C begins to show an isotropic clay matrix [18] [19] [20]. SEM morphological investigations and EDS elemental chemical microanalysis on non-original bricks show a silicon and aluminium based matrix with lower amounts of iron, potassium, magnesium and calcium suggesting a illite/smectite composition. The absence of clay minerals peaks in XRD spectra confirms that clay calcination temperature has been reached. High percentages of diopside detected by XRD have not been observed in optical microscopy. In addition to the rare clinopyroxenes observed in OM, cryptocristalline diopside could be present as product of the reaction between a Mg-rich carbonate (Mg-calcite or dolomite) and quartz. In fact, at 900 °C clinopyroxene occurs according to the reaction [21] [22]:

$$CaMg(CO_3)_2 + 2SiO_2 = CaMgSi_2O_6 + 2CO_2$$

dolomite quartz diopside

The presence of Ca and Mg in non-original bricks was confirmed by EDS elemental chemical analyses carried out on the bulk of non-original samples.

Porosity is another distinguishing feature: it is lower in the original bricks (about 5%) and higher in the non-original ones (10-15%). The porosity decreasing, caused by the sintering process, generally is determined by the sintering temperature and time, but it also depends on the level of the initial porosity and on the raw materials grain size [23].

More diffused porosity in non-original bricks, in spite of the higher firing temperatures, could be attributed to the coarser grain size and to the greater abundance of the a-plastic fraction. In fact in original bricks a-plastic fraction grain size is fine and it does not exceed 125 μm, suggesting that silt-very fine sand was used as aggregate. On the contrary, in non-original bricks the a-plastic fraction is more abundant than in the original ones and coarser size reaches up to 250 μm, i.e. belonging to the fine sand grain size class.

B. Stuccoes

Non-invasive ED-XRF analysis performed on stuccoes allowed to preliminary distinguishing the presence of two different typologies.

Mineralogical and petrographic analyses show that the aggregate has a similar silicate composition in both groups, with a grain size like a poorly sorted fine to coarse sand with silt. On the contrary, binder composition is the main feature that involves the distinction among the stuccoes samples. SEM/EDS analyses detected a carbonate binder with an appreciable amount of Mg only in the original stuccoes (Stucco I: MY3, MY8, MY9, MY14, MY15, MY16 samples). XRD spectra confirm the presence of Mg-calcite.

SEM-EDS, FT-IR and XRD analyses detected gypsum in stucco sample (MY12), which is probably not original (Stucco II: MY11 and MY12 samples).

C. Mortars

The analysed mortars samples are characterized by two different binder typologies. In the original mortars (mortar I: MY7, MY17 samples) neither XRD, nor FT-IR or even TG analyses have detected the presence of calcium carbonate. On the other hand, X-ray diffraction detected a moderate amount of illite (Table 3) Therefore it is possible to assume that mortars were made using a silicate binder (clays). Furthermore, as was in the habit of Pagán specialists, additives of organic origin that somehow has hardened during the drying phase could have been used [24]. This organic binder has not been detected probably because of its complete leaching.

On the contrary, the second type of mortar (mortar II: MY4, MY5, MY6, MY13, MY17.1, MY17.2 samples) shows a mainly carbonate binder associated with a secondary silicate phase, probably consisting of clay minerals. This phase was observed only in EDS spectra, while has not been detected in X-ray diffraction because its percentage is probably lower than the instrumental sensitivity. Mineralogical composition of the aggregate is quite similar in both groups, except for rare hornblende detected by OM and SEM investigations in non-original mortars (low percentages do not allow the detection by XRD). Rock fragments typologies differ into the two groups (limestone in original mortars, quartzite in non-original ones). The two groups differ also for the contents of bioclasts: in fact, shells and frustules can be well observed in original mortars while bioclasts are rare in non-original ones. Furthermore, grog was detected only in original mortars. Rare yttrium particles in association with phosphorous were detected in one non-original sample (MY5) by SEM investigations (fig.11a, 11b).

D. Statistical data treatment

Semiquantitative data offered by the EDXRF spectrometer couldn't be considerate as absolute values, therefore they were considered in a comparative way in order to discern if they are proper enough to perform a grouping model of the Pagoda n. 1205 materials on the base of their elemental composition differences or similarities.

From the score plot reported in fig. 12a quite good separation among the different groups has been achieved. The more homogeneous group is represented by Stucco I group. Bricks (both I and II groups) show the higher concentrations of Si, Fe, K and Ti (see the loading plot in fig.12 b). On the contrary Stucco I group is characterized by the higher Ca content, mainly present as $CaCO_3$ in

accordance with XRD, TGA and FT-IR results. Stuccoes II, (non-original), show the higher concentration in Mn and Zr with respect to the other samples. This is probably due to the use of a different raw material.
In fig. 13 the dendrogram obtained from HCA is reported. The more distinguishable materials are Stuccoes (II), confirming what observable in the score plot. On the contrary bricks II and I groups are more homogeneous probably because they differ only from the grain size. As regards mortars, in accordance with PCA results, we can affirm that the two classes are well distinguishable from the compositional point of view.

CONCLUSIONS

This integrated study allowed to discriminate original and not original materials used in temple n. 1205a in Pagán region. Principal component analysis (PCA) and hierarchical cluster analysis (HCA) performed on EDXRF chemical compositional data allowed to discriminate the different materials.
Two brick typologies were identified, one original and the other related to a restoration intervention. Grain size (silt-very fine sand vs fine sand), porosity (low vs high percentages) and clay matrix optical properties (anisotropy vs isotropy) are the features that allow to distinct the two bricks groups in OPM. The last difference could be related to different thermal treatments for the original vs non-original bricks. In support of this hypothesis, evidences of pyrometamorphic reactions were considered.
Preliminary distinction among the stuccoes was carried out by EDXRF analyses. This distinction between original and restoration material has been confirmed by microscopy and spectroscopy data and by the statistical data treatment.
Binder composition (respectively Mg-carbonate vs gypsum) has been identified as main distinctive marker.
The provenance of Mg-rich raw material could be localised in the Shan State (east of Birmani), where dolomites and dolomitic limestone occupy a vast area of the uplands plateau of the region. In central Birmani gypsum occurs as transparent crystals (selenite) associated with Pegu clays and shales of the Thayetmyo, Minbu, Magwe, Myingyan and Pakokku districts as thin laminae along bedding planes, or as narrow veinlets filling their cracks and joint planes [25].
Concerning sampled mortars, two different binders were found. In the original mortars none of the analyses have detected the presence of $CaCO_3$, suggesting that a silicate binder (clays) and an organic binder (not detected probably because of deterioration) were used. Mortar employed in a probable restoration intervention shows a carbonate binder associated with a silicate phase, probably consisting of clay minerals. Furthermore, in original mortars shells, frustules and grog were observed.
Regarding the a-plastic mineralogical composition the presence of original quartz, orthoclase and plagioclase in both original and non-original is somewhat compatible with a granite/rhyolite composition. Furthermore, coarse fragments of quartzite, present only in non-original bricks, could indicate an origin of raw material from a metamorphic region [26].

It is possible that local river sand was used as raw material for the aggregate. If so, this mineral association could reflect the wide drainage basin of Irrawaddy river, flowing nearby the Pagán site [24]. Evaluated the Irrawaddy drainage basin, two main Burmese geographic provinces with distinctive geological features are considered as potential local sources for the sediment: the Sino-Burman Ranges (including also the Wuntho-Popa Arc and the metamorphic belt rocks that crop out along the ranges) and the Indo-Burman Ranges.

Concerning yttrium particles found in original stucco samples they could be related to xenotime (yttrium orthophosphate $Y(PO_4)$, a mineral present in sands of southern Birmani (Dawei and Myeik regions) which occurs in association with cassiterite deposits. The mineral occurs in pegmatite veins, as a minor accessory mineral in granites and crystalline metamorphic rocks. It is also found as a heavy residual mineral in the sands of streams.

Likewise the trace rare earth elements (REEs) detected in some samples (bricks II and mortars I and II) are related to different deposits located in Mandalay Region [27] [28] and they could represent distinctive elements (markers) to recognize the constitutive materials provenance. In tropical environments such as Birmani, rocks are deeply weathered and the processes of soil formation commonly concentrate heavy elements as residual deposits, resulting in an enriched-metal layer over the underlying, unweather bedrock.

Concerning silver, copper and tin presence, some mines, deposits and ore in the surrounding area could be considerate.

Silver ores mainly occurs in association with lead minerals. Lead-silver deposits of Bawdwin (Northern Shan States) constitute the most important in Burma. Other potential sources are located in regions along the banks of the Irrawaddy River: the silver-lead mines of Penshi (Bhamo District), cerussite veins of Kaydwin (Katha district) and the lode of argentiferous galena among the foothills of Mount Pima (Yamethin District).

Copper occurs in several localities in Burma. In Northern Shan State, chalcopyrite is found disseminated in minute grains through the country rock, occurring in association with galena at Bawdwin. In the extreme south of Myitkyina District, copper ore was extracted from the Taungbalaung reserve, west the first defile of the Irrawaddy. Malachite and chalcanthite were found to occur locally as vein minerals in the rhyolitic agglomerates and tuffs in the Letpandaung hills in the Lower Chindwin District. The veins of the gold mines at Kyaukpazat (Katha District) carry five per cent of chalcopyrite, pyrite, galena and franklinite.

Cassiterite and wolfram, the most important tin-bearing minerals, occurs in Southern Birmani (Mergui, Tavoy, Amherst, Thaton Districts) [29].

REFERENCES

[1] D. M. Statdner, Sacred sites of Burma, River Books, 2011, pp. 214-230.

[2] J.C. Yarmola, Conservation of Historic Brick Masonry in Pagán , Restricted, UNDP/ BUR/78/023 Technical Report, United Nations Development Programme, Paris, 1987.

[3] Post-earthquake Damage Assessment Survey of Cultural Heritage Buildings at Pagán Archaeological Zone – Quick Report, Tokyo National Research Institute for Cultural Properties, December 2016.
[4] Me-taw-ya Pagoda Project - Capacity Building; a Conservation Project for the Repair, Strengthening and Recovery of Temple 1205. Archaeological Area and Monuments of Pagán , Burma 2016 – 2020 Draft report 2018, Tokyo National Research Institute for Cultural Properties (TRICP).
[5] A.H.G Mitchell, Cretaceous–Cenozoic tectonics events in the western Birmani (Burma) Assam region. Journal of the Geological Society 150, 1993, pp. 1089–1102.
[6] K. Khin, Myitta, Marine transgression and regression in Miocene sequences of northern Pegu (Bago) Yoma, Central Birmani. Journal of Asian Earth Sciences, Volume 17, Issue 3, 1999 pp. 369-393.
[7] I. Metcalfe, Tectonic framework and Phanerozoic evolution of Sundaland. Gondwana Research 19, 2011, p. 3–21.
[8] F. Bender, Geology of Burma. Borntraeger, Berlin, 1983.
[9] G. Bertrand, C. Rangin, Tectonics of the western margin of the Shan plateau (central Birmani): implication for the India–Indochina oblique convergence since the Oligocene. Journal of Asian Earth Sciences 21, 2003, pp. 1139–1157.
[10] A.H.G. Mitchell, M. Thein Htay, K. Min Htun, M. NaingWin, T. Oo, T. Hlaing, Rock relationships in the Mogok metamorphic belt, Tatkon to Mandalay, central Birmani. Journal of Asian Earth Sciences 29, 2007, pp. 891–910.
[11] K. Zaw, Geological, petrological and geochemical characteristics of granitoid rocks in Burma: with special reference to the associated W-Sn mineralization and their tectonic setting. Journal of Southeast Asian Earth Sciences Volume 4, Issue 4, 1990, pp. 293-335.
[12] A. Mitchell, Sun-Lin Chung, Thura Oo, Te-Hsie Lin, Hung, Chien Hui Hung, Zircon U–Pb ages in Birmani: magmatic–metamorphic events and the closure of a neo-Tethys ocean? Journal of Asian Earth Sciences 56, 2012, pp.1–23. DOI: 10.1016/j.jseaes.2012.04.019.
[13] L. Ma, Y. Wang, W. Fan, H. Geng, Y. Cai, H. Zhong, H. Liu, X. Xing, Petrogenesis of the early Eocene I-type granites in west Yingjiang (SW Yunnan) and its implication for the eastern extension of the Gangdese batholiths. Gondwana Res., 25, 2014, pp. 401–419.
[14] J. Wang, F. Wu, X. Tan, C. Liu, Magmatic evolution of the Western Birmani Arc documented by U-Pb and Hf isotopes in detrital zircon. Tectonophysics, 2014, pp. 612–613, pp. 97–105.
[15] T. Maurin, C. Rangin, Structure and kinematics of the Indo-Burmese Wedge: recent and fast growth of the outer wedge. Tectonics, 28 (2), 2009. DOI: 10.1029/2008TC002276.
[16] A. R. Philpotts, Petrography of igneous and metamorphic rocks, Englewood Cliffs, N.J: Prentice Hall, 1989.
[17] J. Gadsden, Infrared Spectra of Minerals and Related Inorganic Compounds, Printed and bound by Acford Ltd, Ed. Butterworths A. London, 1975, p. 277.
[18] J.D Seger, Retrieving the Past: Essays on Archaeological Research and Methodology in Honor of Gus W. Van Beek, Eisenbrauns, 1996, p. 312.
[19] S.J. Vaughan, Ceramic Petrology and Petrography in the Aegean, Am. J. Arch. 99 (1), 1995, pp. 115-117.

[20] C.A. Rice, Process for surface treating clay minerals and resultant products. U.S. Patent No 4,690,868, 1987.
[21] H.G.F. Winkler, Petrogenesis of metamorphic rocks, Springer-Verlag New York, 1979, pp. 348. DOI 10.1007/978-1-4757-4215-2.
[22] R. Grapes, Pyrometamorphism, Springer Berlin Heidelberg New York, 2006 pp. 199
[23] C. Barry Carter, M. Grant Norton, Sintering and Grain Growth. In: Ceramic Materials. Springer, New York, 2007, pp 427-443. DOI 10.1007/978-0-387-46271-4_24.
[24] J.C. Yarmola, Conservation of Historic Brick Masonry in Pagán. Report prepared for the Socialist Republic of the Union of Burma by UNESCO, Paris, 1987.
[25] J. Coggin Brown, Mineral Wealth: Part III. Materials used in building construction, civil engineering, etc. Gyan Publishing House, 1955, p. 761.
[26] H.L. Chibber, "The Geology of Burma", MacMillan and Co, London, 1934, p. 530.
[27] K. M. Kyu, Y. Y. Myint, S. Yee, The study of the Elemental Concentration in Some Rocks and Cements in Birmani, Jour. Myan. Acad. Arts & Sc. Vol III N. 3 (1) Physics, 2005, pp. 107- 119.
[28] A. T. Tara, T. Z. Myob, T. M. Hlaingc, B. B. M. Wind, Study on Processing of Rare Earth Oxide from Monazite, Mongmit Myitsone Region, American Scientific Research Journal for Engineering, Technology, and Sciences (ASRJETS), Vol 27, N. 1, 2017, 43-51, pp. 2313-4410.
[29] H.L. Chibber, The mineral resources of Burma, MacMillan and Co, London, 1934, p. 320.

Figure 1

Click here to download high resolution image

Figure 2

Click here to download high resolution image

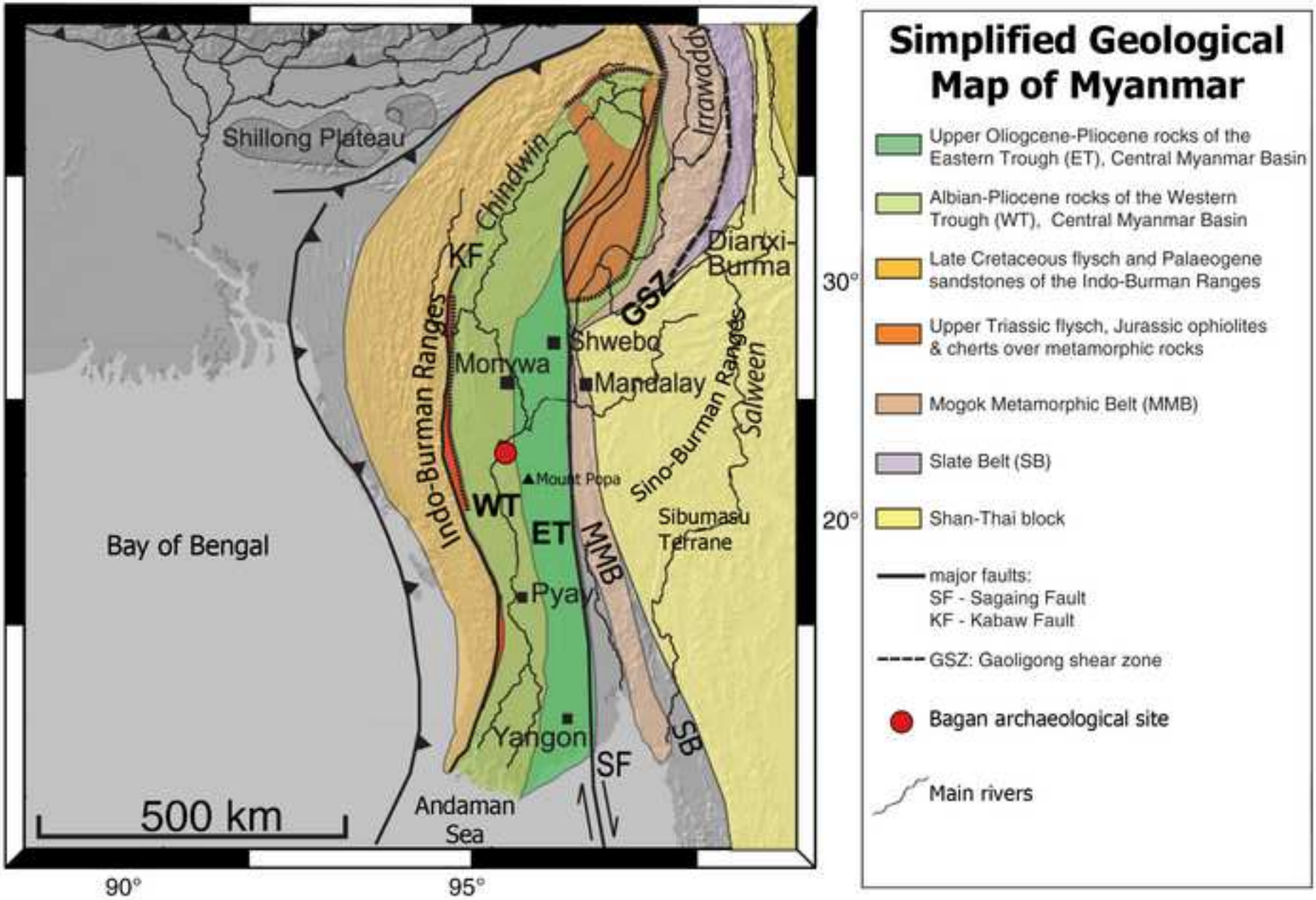

Figure 3

Click here to download high resolution image

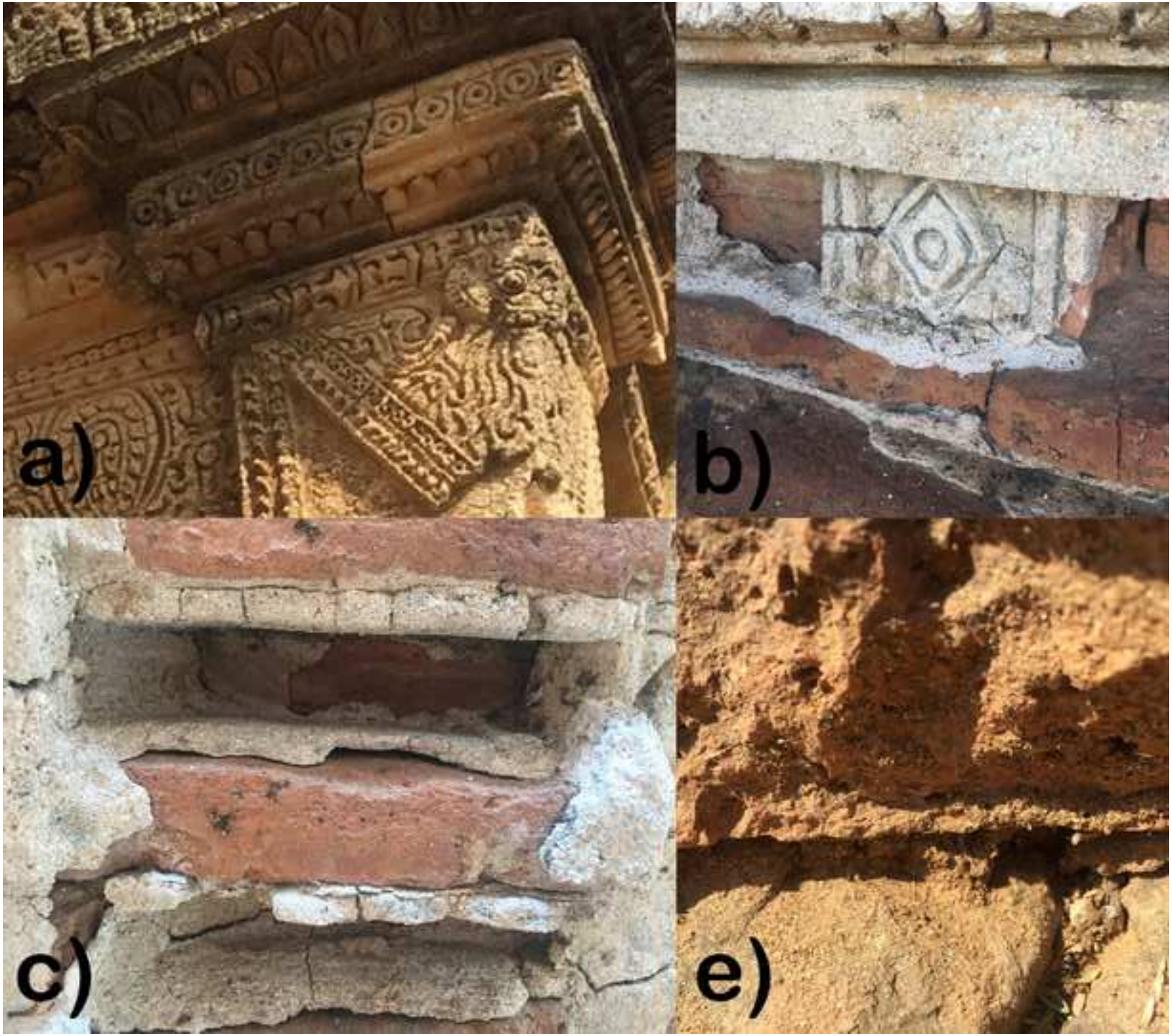

Figure 4

Click here to download high resolution image

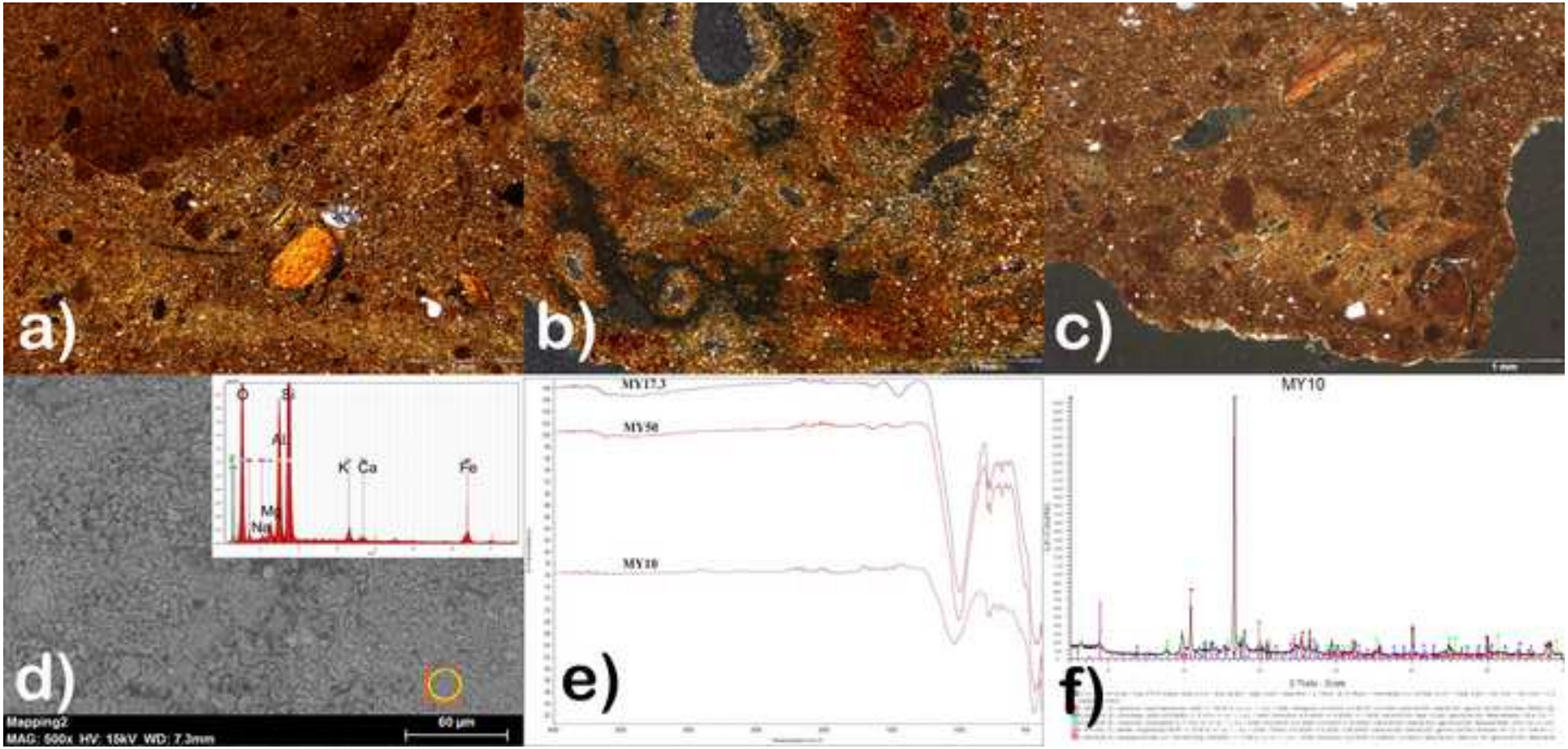

Figure 5

Click here to download high resolution image

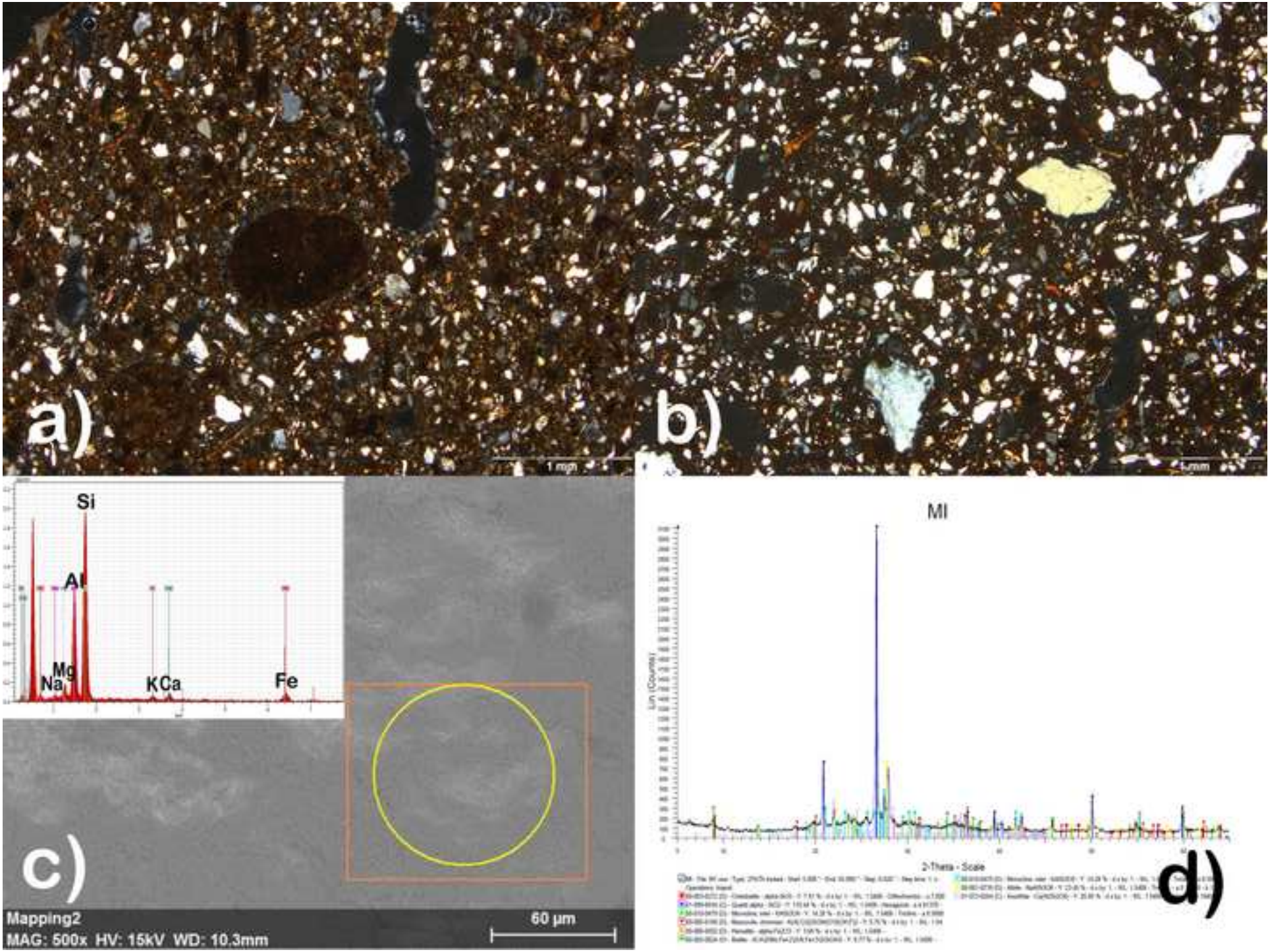

Figure 6

Click here to download high resolution image

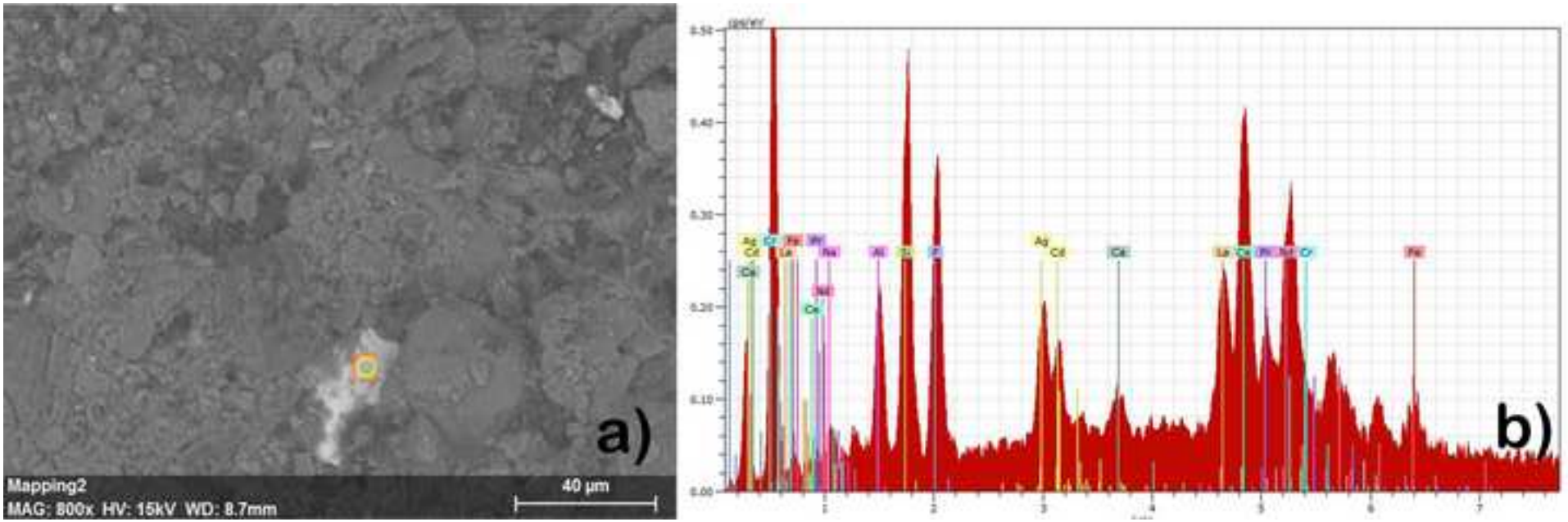

Figure 7

Click here to download high resolution image

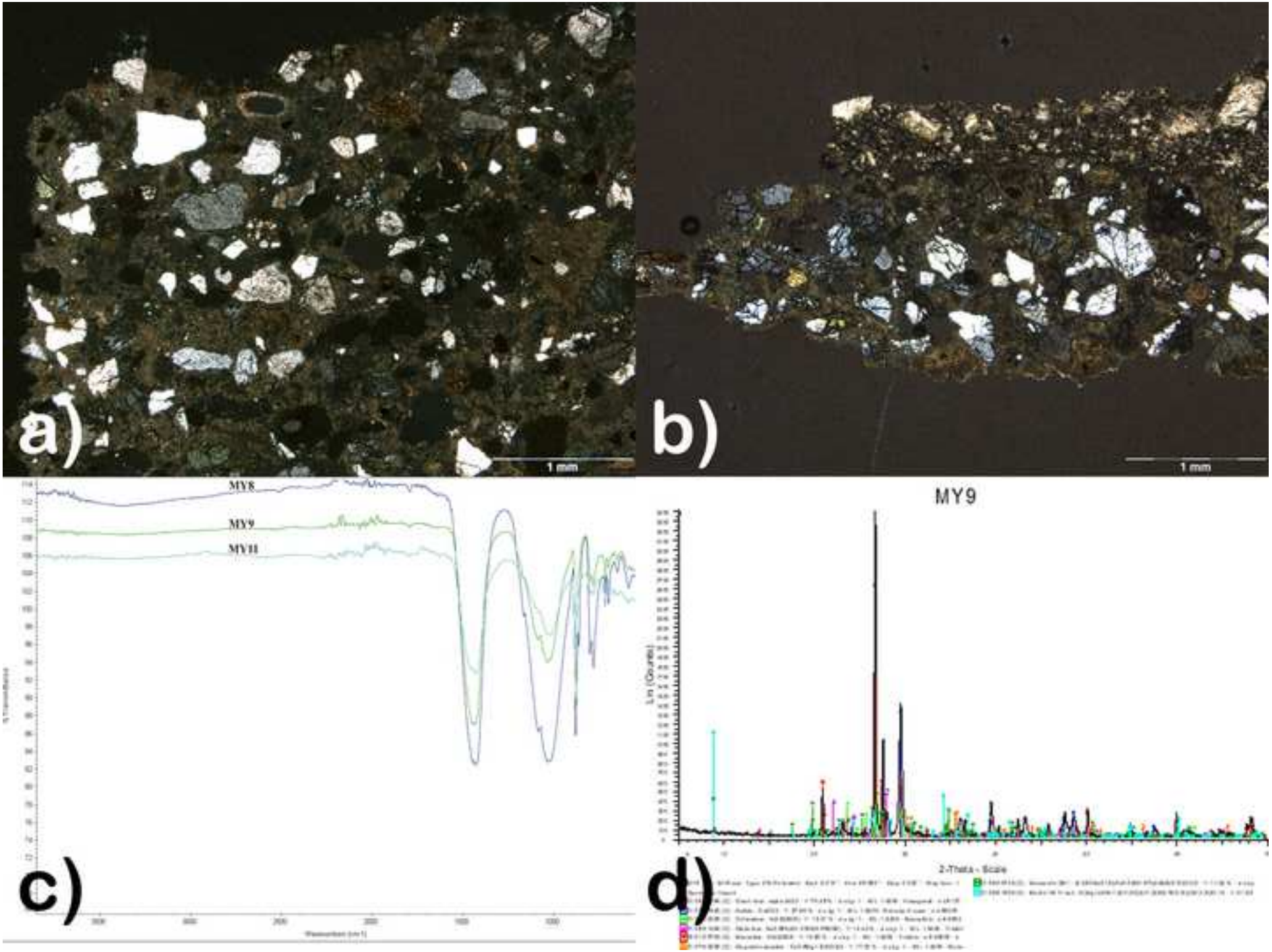

Figure 8

Click here to download high resolution image

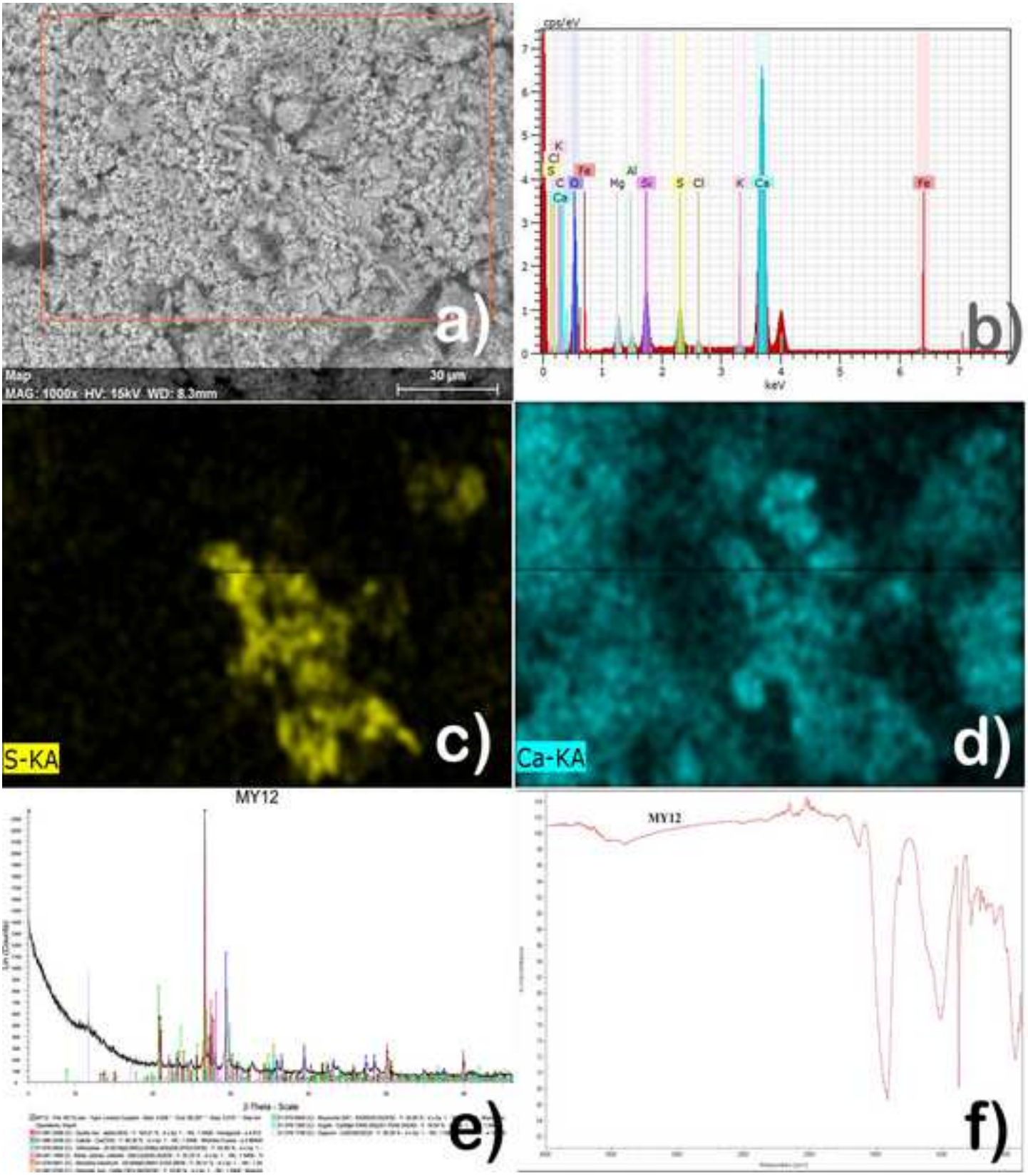

Figure 9

Click here to download high resolution image

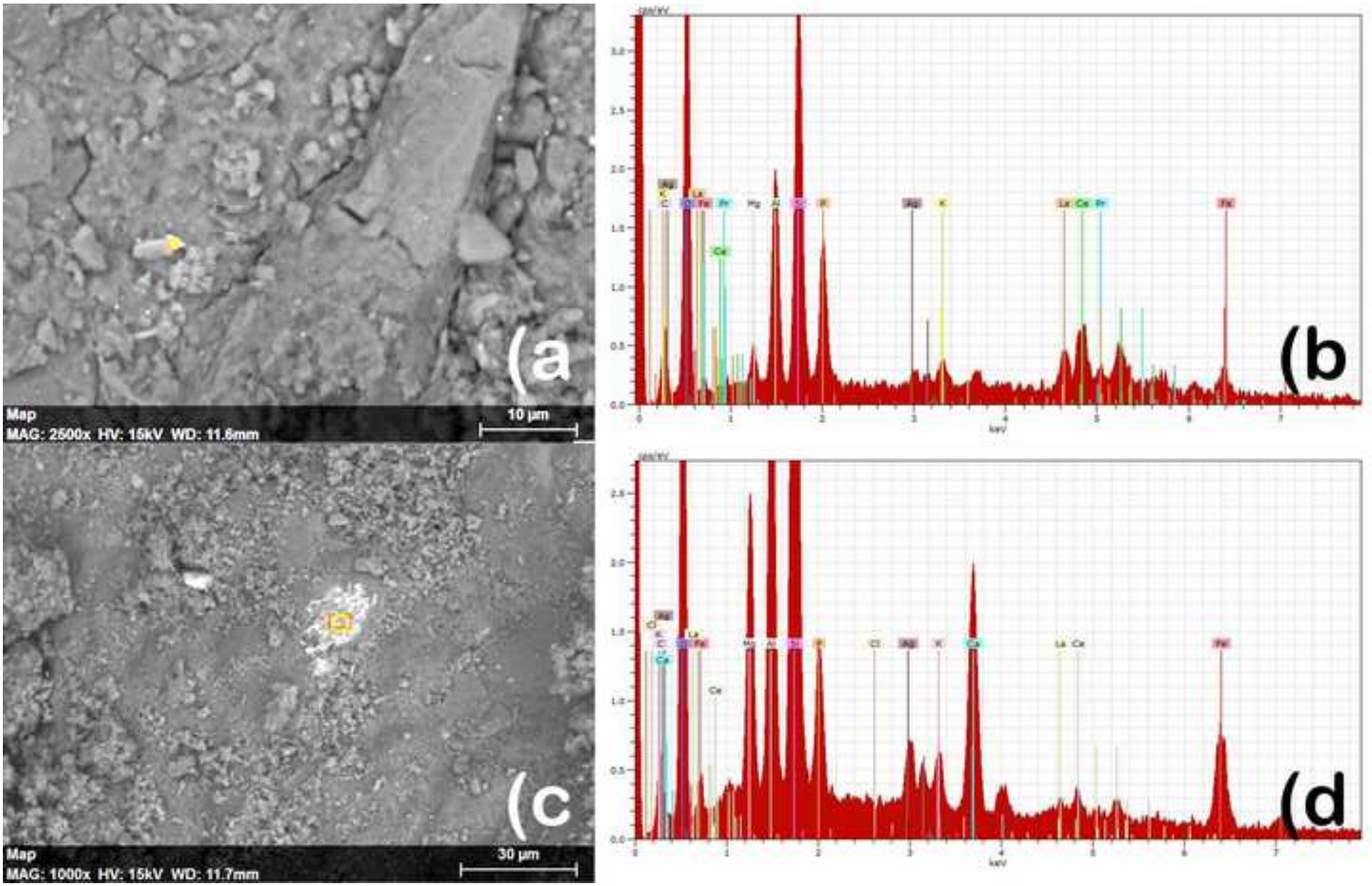

Figure 10

Click here to download high resolution image

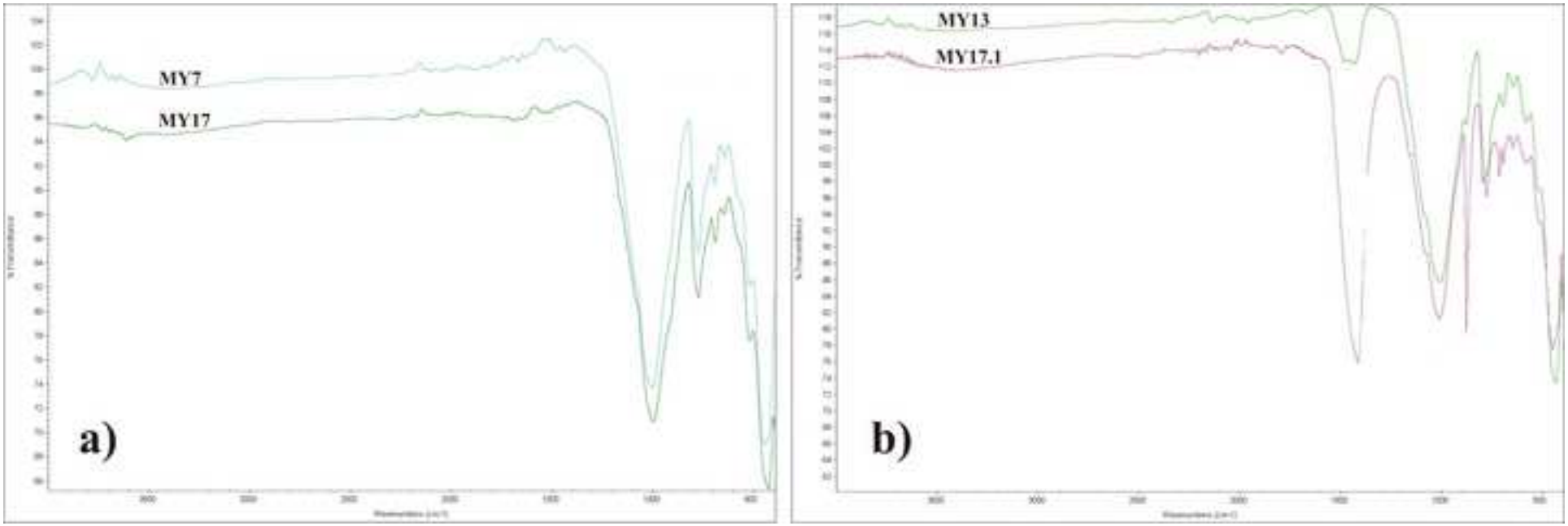

Figure 11

Click here to download high resolution image

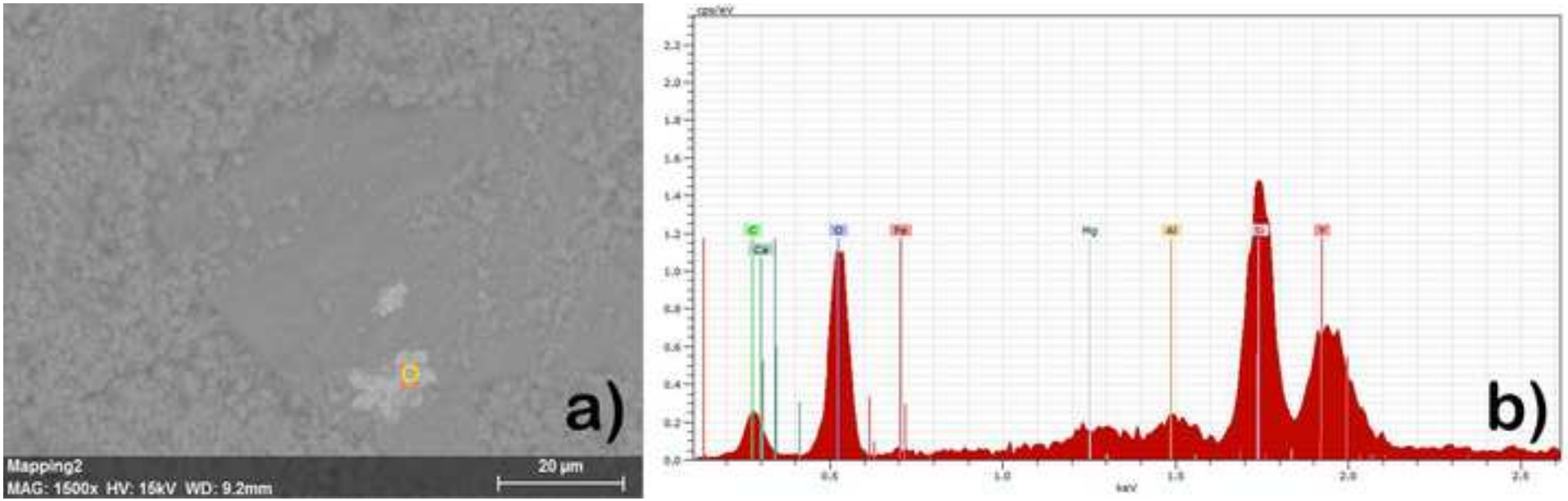

Figure 12

Click here to download high resolution image

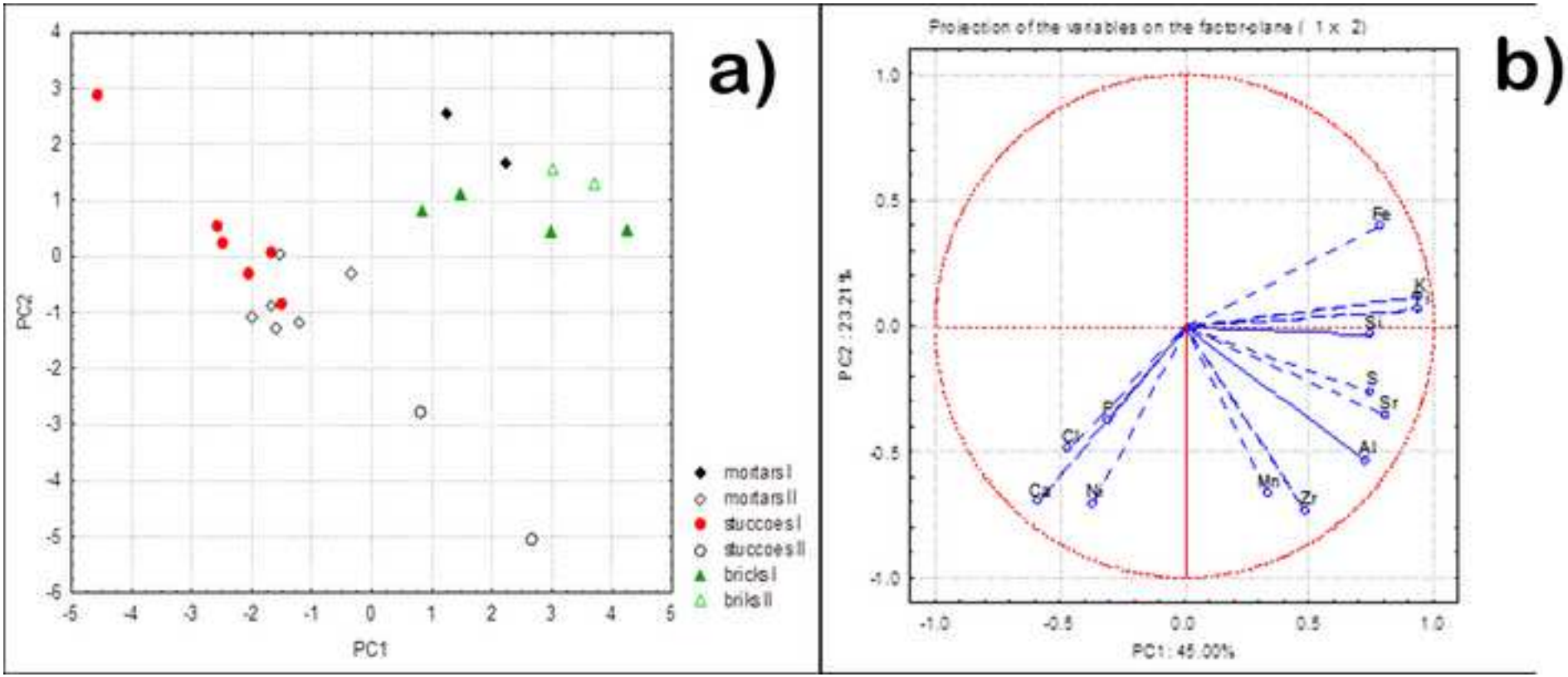

Figure 13

Click here to download high resolution image

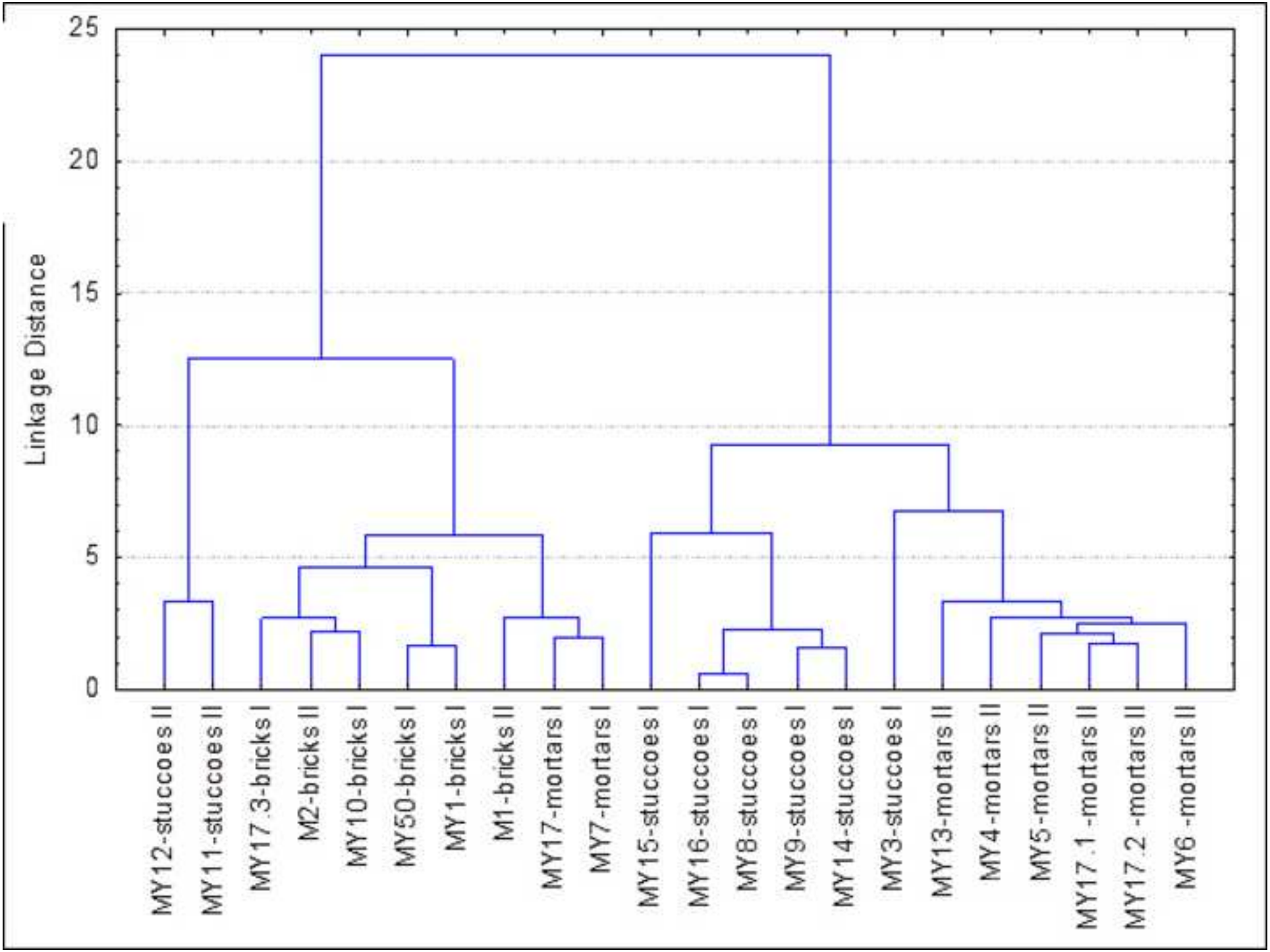

FIGURES CAPTIONS

Fig. 1. Temple n. 1205a from Bagan Archaeological Area

Fig. 2. Myanmar Geological Map

Fig. 3 Sampling areas: a) MY8, MY9 samples; b) MY11, MY12 samples; c) MY14, MY15 samples; d) MY7 sample

Fig. 4. Brick I samples: a) MY1, 2,5x, nicols X, transmitted light; b) MY10, 2,5x, nicols X, transmitted light; c) MY17.3, 2,5x, nicols X, transmitted light; d) SEM-EDS of MY1 matrix area; e) FT_IR; f) MY10, XRD spectrum.

Fig. 5. Brick II samples: a) M1, 2,5x, nicols X, transmitted light; b) M2, 2,5x, nicols X, transmitted light; c) SEM-EDS of M2 matrix area; d) e) M1, XRD spectrum.

Fig. 6 SEM-EDS of M1 sample (brick II) showing the presence of rare earths. SEM micrograph (a); EDS spectrum (b)

Fig.7. Stucco I samples: a) MY14, 2,5x, nicols X, transmitted light; b) MY15, 2,5x, nicols X, transmitted light; c) FT-IR spectra; d) MY9, XRD spectrum

Fig.8. Stucco II sample MY12: a) SEM micrograph; b) SEM spectrum; c) Sulphur EDS elemental map; d) Calcium EDS elemental map; e) MY12, XRD spectrum; f) MY12, FT-IR spectrum

Fig. 9 SEM-EDS micrographs and spectra of rare earths in mortar samples: a/b) MY7 sample (mortar I); c/d) MY17.1 sample (mortar II)

Fig. 10. FT-IR spectra: a) My7 and My17 samples (mortar I); (b) My13 and My17.1 samples (mortar II)

Fig. 11. MY5 stucco sample: (a) SEM micrograph and (b) EDS spectrum showing the presence of yttrium particle

Fig. 12. Score plot a) and loading plot b) obtained from PCA analysis carried out on the entire data set of samples (mortars, stuccoes and bricks); PC1 and PC2 account for about 70% of total variance.

Fig. 13. HCA obtained for the entire data set of samples (mortars, stuccoes and bricks).

Table 1

Sample Code	Sample description
MY1	Red brick
MY2	Joint mortar
M1	Red brick
M2	Red brick
MY3	Grey outer stucco
MY4	Whitish outer mortar
MY5	Whitish outer mortar
MY6	Grey joint mortar
MY7	Joint mortar
MY8	Whitish outer stucco
MY9	Inner stucco
MY10	Red brick
MY11	Inner stucco
MY12	Whitish outer stucco
MY13	Joint mortar
MY14	Inner stucco
MY15	Inner and outer stucco
MY16	Whitish outer stucco
MY17	Joint mortar
MY 17.1	Joint mortar
MY 17.2	Joint mortar
MY 17.3	Red brick
MY50	Red brick

Table 2

Group	Sample	I/M/P	Relative abundance of inclusions					Main mineralogical composition of inclusions			Groundmass
			<63 μm	63-125 μm	125-250 μm	250-500 μm	>500 μm	< 125 μm	125-250 μm	> 250 μm	
Mortars II	MY4	25:70:5	+++	+++	++	+	+	Qz, Opq, Cpx	Qz, Crs, Kfs, Pl, Cpx, Amp, Opq, CRF	Qz, Kfs, MRF,	A
	MY5	20:70:10	++	++	+++	++	+	Qz, Opq, Cpx	Qz, Pl, Kfs Amp, Cpx, Grt, Opq, CRF	Qz, Pl, Crs, MRF,	A
	MY6	20:65:15	++	++	++	+++	+++	Qz, Cpx, Opq, Bt, Ms, Amp, Ttn	Qz, Kfs, Pl, Cpx, Ep, CRF	GR, Qz, Kfs, Bt, CRF	A
	MY 17.1	20:75:5	±	+	++	+++	++	Qz, Kfs, Cpx, Bt, Ms	Qz, Kfs, Pl, Cpx, Amp, Opq, Ms, Bt	Qz, Kfs, Cpx, Pl, Amp, Opq, LRF, MRF, BC	A
Stuccoes I	MY3	25:70:5	++	++	+++	++	±	Qz, Opq, Cpx,	Qz, Pl, Kfs, Crs Amp, Opq	Qz, Grt, MRF	A
	MY9	25:65:10	++	++	+++	++	±	Qz, Cpx, Ms, Bt, Opq,	Qz, LRF, Kfs, Pl, Cpx, Bt, Amp	Qz, Kfs, MRF	A
	MY14	25:70:5	+	++	+++	+++	++	Qz, Cpx, Opq	Qz, Kfs, Pl, Cpx, Ms, Bt, Opq	Qz, Kfs, Pl, Cpx, MRF, Ms, Amp	A
	MY15	25:70:5	±	++	+++	+	±	Qz, Cal, Cpx, Opq	Qz, Cal, Cpx, Amp, Pl	Qz, Cal, Kfs, Bt, Cpx, MRF	A
Bricks I	MY1	10:85:5	+++	+	±	±	tr.	Qz, Bt, Ms, Kfs, Opq, Cpx, Ap	ARF, Bt, Qz	Bt	A
	MY10	5:80:15	+++	±	±	tr.	-	Qz, Ms, Bt, Opq, Cpx	Qz, Kfs, Cpx	Qz	A/SI
	MY 17.3	5:85:10	+++	+++	+	±	-	Qz, Ms, Bt	Qz, Bt, Kfs, Amp, Ep	Qz	A/SI
Bricks II	M1	20:70:10	++	+++	++	±	±	Qz, Pl, Kfs, Bt, Crs, Ms, Amp, Opq	MRF, Qz	ARF	SI
	M2	25:65:15	++	+++	+	±	±	Qz, Pl, Bt, Kfs, Crs, Opq, Ms, Amp	Qz	MRF, Qz	SI

Table 3

	Pl	*Cpx*	*Cal*	*Chl*	*Gy*	*Qtz*	*Kfs*	*I/M*
MORTAR I (joint mortar)								
MY7	xx			x		xxxx	±	x
MY17	x			x		xxxxx	±	x
MY2B	x			x		xxxxx	±	x
MORTAR II								
MY6	xx	x	xxx			xxxx	x	xx
MY13	x	x	xx			xxxx	±	xx
MY17.1	x	x	xx			xxxxx	x	±
MY17.2	x		x	±		xxxx		x
MY4	x		x			xxxxx	x	±
MY5	x		xx			xxxx	x	
STUCCO I								
MY3 outer	xx		xx			xxxxx	x	x
MY8 outer	x		x			xxxx	xx	±
MY9 inner	x	x	xx			xxxx	x	x
MY14 inner	x	x	xx			xxxx	x	x
STUCCO II								
MY11 inner	x	±	xx			xxxx	x	x
MY12 outer	x	x	xx		x	xxxx	xx	x
BRICK I								
MY1				x		xxxx		x
MY50						xxxx		xx
MY17.3				x		xxxx		xx
MY10						xxxx		x
BRICK II								
M1	x					xxxx		xxxx
M2	x					xxxx		x

Mineral name's abbreviations, Pl= plagioclase, Cpx = clinopyroxene, Cal= Calcite, Chl=Chlorite, Gy= gypsum, Qtz = quartz, Kfs = K-feldspar, I/M = illite/miche.
Semi-quantitative estimate/ +++=very abundant; ++=abundant; +=lowly abundant; ±=scarce; tr=traces.

TABLES CAPTIONS

Table 1. Sample list collected from Temple n. 1205a.

Table 2. Minero-petrographic description of the samples. I/M/P = inclusions, matrix and pores percentages. Mineral name's abbreviations: Amp = amphibole, Ap = apatite, Bt = biotite, Cal = calcite, Cpx = clinopyroxene, Crs = cristobalite, Ep = epidote, Grt = garnet, Kfs = K-feldspar, Ms = muscovite, Opq = opaque minerals, Pl = plagioclase, Qz = quartz, Ttn = titanite.
Other inclusions abbreviation: ARF = argillaceous rock fragments; CRF = calcareous rock fragments; MRF = metamorphic rock fragments; GR = Grog. Semi-quantitative estimate: XXX=very abundant; XX=abundant; X=lowly abundant; ± = scarce; Tr.= traces. A = anisotropic, SI = semi-isotropic.

Table 3. XRD analysis performed on samples, highlighting the groups.

Table 1s. XRF analysis, mean values.

Table 1s

Click here to download Supplementary Material: TABLE 1s.docx